Journal of Power Sources 196 (2011) 9027–9035

Contents lists available at ScienceDirect

Journal of Power Sources

journal homepage: www.elsevier.com/locate/jpowsour

Experimental and computational investigations of a compact steam reformer for fuel oil and diesel fuel

M. Grote[a,*], M. Maximini[a], Z. Yang[a], P. Engelhardt[a], H. Köhne[a], K. Lucka[a], M. Brenner[b]

[a] OWI Oel-Waerme-Institut GmbH, An-Institut RWTH Aachen, 52134 Herzogenrath, Germany
[b] Behr GmbH & Co. KG, 70469 Stuttgart, Germany

ARTICLE INFO

Article history:
Received 31 October 2010
Received in revised form
18 November 2010
Accepted 23 November 2010
Available online 1 December 2010

Keywords:
Steam reforming
Fuel oil
Diesel fuel
CFD computation

ABSTRACT

The present work describes the optimisation of a compact steam reformer for light fuel oil and diesel fuel. The reformer is based upon a catalytically coated micro heat exchanger that thermally couples the reforming reaction with a catalytic combustion. Since the reforming process is sensitive to reaction temperatures and internal flow patterns, the reformer was modelled using a commercial CFD code in order to optimise its geometry. Fluid flow, heat transfer and chemical reactions were considered on both sides of the heat exchanger. The model was successfully validated with experimental data from reformer tests with 4 kW, 6 kW and 10 kW thermal inputs of light fuel oil. In further simulations the model was applied to investigate parallel flow, counter flow and cross flow conditions along with inlet geometry variations for the reformer. The experimental results show that the reformer design allows inlet temperatures below 773 K because of its internal superheating capability. The simulation results indicate that two parallel flow configurations provide fast superheating and high fuel conversion rates. The temperature increase inside the reactor is influenced by the inlet geometry on the combustion side.

1. Introduction

Fuel cell systems comprising of PEM fuel cells and steam reformers have high potential as stationary or mobile auxiliary power units. In particular, the use of liquid fossil fuels with an existing infrastructure like fuel oil and diesel fuel promises an early economic breakthrough of the technology.

The implementation of steam reformers in the power range up to 20 kW for domestic fuel oil or diesel fuel as a catalytically coated plate heat exchanger or micro channel heat exchanger has advantages over other reactor concepts. In comparison to a shell and tube heat exchanger the micro channel and plate heat exchanger provides higher heat flow densities. A technical application for methane steam reforming based on a plate heat exchanger with wavy plates was developed by Gritsch [1]. The reformer has a volume of 0.7 l and provides up to 15 kW hydrogen at reactor temperatures up to T = 1173 K. Kolb et al. [2] developed a micro channel heat exchanger for steam reforming of diesel fuel. Operating temperature is T = 1073 K. The reactor with a volume of 0.25 l generates 2 kW hydrogen. On the burner side of the reactor anode exhaust gas is catalytically burnt. Another application for diesel fuel steam reforming is a reactor with S-shaped micro channels developed by Thormann [3]. The reactor is designed for a fuel input of 0.2 kW. Hydrogen is supplied to the burner side.

The steam reformer examined in this work is designed as a catalytically coated micro channel heat exchanger. Therein, the endothermic steam reforming process of light fuel oil is heated by the exothermic catalytic combustion process. The reactive flows are conducted through parallel channels. The steam reformer was built up as a full scale reactor and a small scale reactor. The full scale reactor with a volume of 0.68 l and a fuel input of 10 kW fuel (hydrogen output of 12 kW) was used for system testing. In the present study the reactor was scaled down to 1 kW. The small scale reactor is based on the same heat exchanger is used to perform a detailed test program. Within another experimental investigation variants of the scaled down reactor are applied to a catalyst screening and geometry optimisation. In the framework of reactor development and improvement CFD computations of the reactor are performed and the results will be discussed in detail in this paper.

2. Theory and modelling

2.1. Steam reforming

Fuel oil and diesel fuel consist of a large number of higher hydrocarbons. A number of investigations have shown that the steam reforming of higher and lower hydrocarbons can be modelled by

* Corresponding author at: OWI Oel-Waerme Institut GmbH, Simulation, Kaiserstr. 100, 52134 Herzogenrath, Germany. Tel.: +49 2407 9518118; fax: +49 2407 9518223.
E-mail address: M.Grote@owi-aachen.de (M. Grote).

0378-7753/$ – see front matter © 2010 Elsevier B.V. All rights reserved.
doi:10.1016/j.jpowsour.2010.11.136

Nomenclature

a, b, c, d	exponents of reaction rates
a^*	coefficient for calculation of effectiveness factor [14]
C	molar concentration of species (mol m^{-3})
E_a	activation energy (J mol^{-1})
k_0, k_1	rate constant of reforming reaction (mol kg (catalyst)$^{-1}$ s^{-1} (mol m^{-3})$^{-(a-b)}$)
$k_0{}^*$	rate constant of reforming reaction corrected by catalyst activity (mol kg^{-1} (catalyst) s^{-1} (mol m^{-3})$^{-(a-b)}$)
k_3	rate constant of combustion reaction (mol kg (catalyst)$^{-1}$ s^{-1} (Pa)$^{-(c+d)}$)
k_b	rate constant of backward shift reaction (mol kg (catalyst)$^{-1}$ s^{-1} (mol m^{-3})$^{-2}$)
k_f	rate constant of forward shift reaction (mol kg (catalyst)$^{-1}$ s^{-1} (mol m^{-3})$^{-2}$)
K_p	equilibrium constant of shift reaction
p	partial pressure of species (Pa)
R	universal gas constant (J mol^{-1} K^{-1})
r_1, r_2, r_3	reaction rates (mol kg (catalyst)$^{-1}$ s^{-1})
r_{eff}	observed rate of reaction (mol kg (catalyst)$^{-1}$ s^{-1})
r_s	rate of reaction at exterior catalyst surface condition (mol kg (catalyst)$^{-1}$ s^{-1})
S, S_0	density of active sites on catalyst of used (partially deactivated) and fresh catalyst (kg (catalyst)$^{-1}$)
X	conversion of fuel
X_r	conversion of fuel at reference point conditions
X_1, X_2, X_3, X_4	conversion of fuel at variation point conditions
α	catalyst activity
η	effectiveness factor
ζ_s	sulphur content of fuel (wt. ppm)
Φ^*	normalised Thiele modulus [14]

a steam reforming reaction to carbon monoxide and hydrogen. In literature two types of equilibrium reactions have been proposed: methanisation or methane steam reforming and CO shift reaction [4–7]. Since the temperatures in the reactor exceed 973 K the formation of methane is not supported by equilibrium. According to the studies of Thormann [3] the steam reforming process can be modelled by the following two reaction steps:

$$C_nH_m + nH_2O \rightarrow nCO + (n + m/2) \quad (\Delta H^0_{298} < 0) \tag{1}$$

$$CO + H_2O \leftrightarrow CO_2 + H_2 \quad (\Delta H^0_{298} = -41\ \text{kJ mol}^{-1}) \tag{2}$$

The steam reforming kinetics of heptane on a Ni/MgO catalyst was examined by Tottrup and Rostrup-Nielsen [8,9]. Thormann determined a power law reaction rate for hexadecane on a ruthenium based catalyst [3]. The corresponding rate equation which was used in this work for reaction (1) is given by:

$$r_1 = k_1 C^a_{C_nH_m} C^{-b}_{H_2} \tag{3}$$

$$k_1 = k_0 \exp\left[\frac{-E_a}{R}\left(\frac{1}{T} - \frac{1}{T_0}\right)\right] \tag{4}$$

The reaction rate constant k_0 is adjusted by subject to the activity of the catalyst coating.

Assuming that CO shift reaction is not limited by kinetic effects, an equilibrium reaction rate can be used for reaction (2):

$$r_2 = k_f C_{CO} C_{H_2O} - k_b C_{H_2} C_{CO_2} \tag{5}$$

$$k_b = \frac{k_f}{K_P} \tag{6}$$

$$K_P = 4290.1 \exp\left(\left(\frac{1\,\text{K}}{T} - 0.001\right) 1.4664\right) \tag{7}$$

The equilibrium constant K_p was fitted in the temperature range between 673 K and 1273 K.

2.2. Combustion

There are two types of reactions which can occur in a catalytic combustion reactor: homogenous and heterogeneous (catalytic). Homogenous reactions occur in the bulk phase while heterogeneous reactions occur on the catalyst surface [10]. A reaction scheme composed of four reaction steps, two heterogeneous and two homogenous reactions, was purposed for a methane catalytic combustion reactor model by Hayes and Kolaczkowski [10]. The gas phase reactions consist of an oxidation reaction of methane to CO and oxidation of CO. The heterogeneous reactions were defined by the oxidation reactions of methane and CO to CO_2. Applying this reaction scheme to the catalytic combustion of higher hydrocarbon leads to unsolved problems since reduced reaction mechanism of homogenous combustion can not reproduce the point of ignition for all conditions. Beyond that Pfefferle and Pfefferle [11] pointed out that the catalyst may also promote homogeneous combustion in the boundary layer by production of gas-phase free radicals. For this reason the combustion is modelled by one overall heterogeneous reaction rate reproducing reaction characteristics from homogenous to heterogeneous combustion:

$$C_nH_m + (n + m/4)O_2 \rightarrow nCO_2 + (m/2)H_2O \quad (\Delta H^0_{298} > 0) \tag{8}$$

Yao [12] investigated the oxidation of alkanes over noble metals. The kinetics of the reaction was treated with a simple empirical law model:

$$r_3 = k_3 p^c_{O_2} p^d_{C_nH_m} \exp\left[\frac{-E_a}{RT}\right] \tag{9}$$

The given values for a platinum based catalyst and butane is used in the implemented model. The constant is adjusted by experiments performed on a monolithic catalyst.

2.3. Mass transfer

In the present case the reaction rates at the catalyst surface are influenced by film diffusion and diffusion in the porous catalyst with a thickness of 25 μm. However, precalculations show that the limitation of heat transfer in the catalyst does not exist. To consider the diffusion in the film by CFD computation a proper resolution of the channels is necessary. The mass transfer in the porous catalyst can be modelled by two different methods. The first option is to determine the concentration profiles in the porous media by for example the dusty gas model [13] which describes the mass transfer in the catalyst. Due to the low catalyst thickness the applied model was derived from the second method: the effectiveness factor concept. In this case the catalyst phase is not considered and the influence of internal mass transfer on the reaction rate can be described by an intrinsic effectiveness factor η which is given by:

$$\eta = \frac{r_{eff}}{r_s} \tag{10}$$

Gottifredi et al. [14] developed a method for estimating the effectiveness factor for many kinetic expression, geometry and site activity distribution. Applying this model to the present case the intrinsic effectiveness factor η is calculated using the expression proposed by [14]:

$$\eta = [\Phi^{*2} + \exp(-a^*\Phi^{*2})]^{-0.5} \tag{11}$$

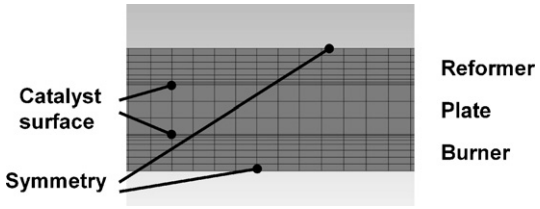

Fig. 1. Reactor model.

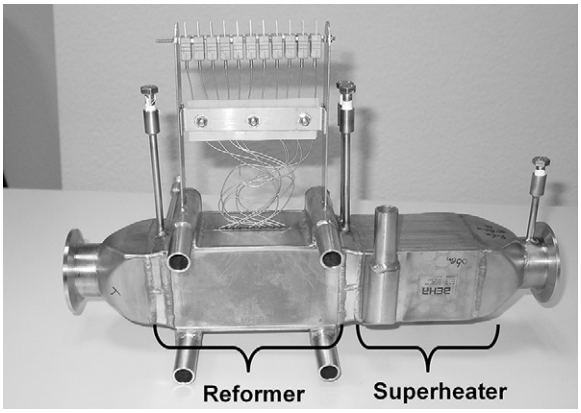

Fig. 2. Steam reformer with superheater.

2.4. CFD computation

The models described in the previous chapters are implemented in the commercial CFD-code ANSYS® CFX 11.0 [15]. In the framework of reactor optimisation numerical calculations of the reactor are performed.

By neglecting heat losses at top plates it is possible to reduce the reactor model to one plate with two half channels and symmetry plane (see Fig. 1).

The reactions are considered by implemented specific species sources at the catalyst surfaces. Surrogate fuel tetradecane was applied to all computations representing fuel oil.

3. Experimental

3.1. Steam reforming reactor 10 kW

The steam reforming reactor was designed as a catalytically-coated plate heat exchanger to couple the endothermic SR reaction with an exothermic catalytic combustion (see Fig. 2). Fig. 3 shows the solid phase temperature measurements points installed in a central plate. The generated reformate has to be cooled down behind the reformer in order to provide optimum inlet temperatures for the downstream high temperature shift reactor (HTS).

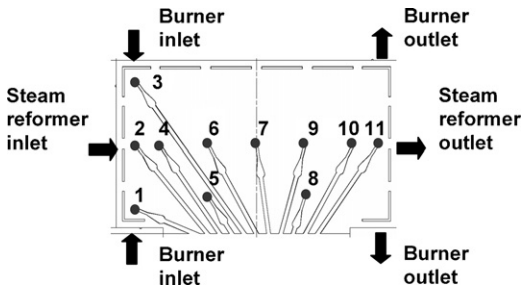

Fig. 3. Temperature measurement plate.

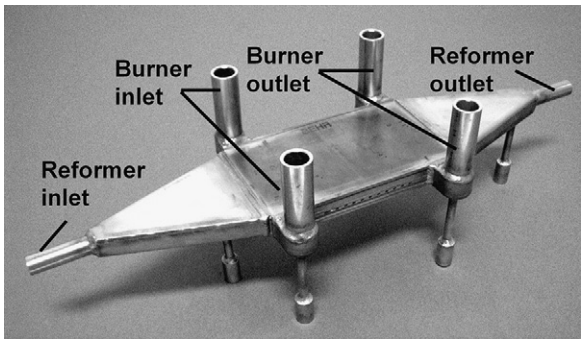

Fig. 4. Small scale reformer.

Therefore another heat exchanger was integrated into the component in order to utilise the reformate heat to superheat the steam before entering the reformer. In addition to the HTS further gas clean-up stages were installed downstream of the reformer to achieve the CO-concentrations required for polymer fuel cells. Fuel-mixture generation on the combustion side was carried out in a cool flame reactor. Therein fuel is injected by a nozzle and mixed with air. Low temperature oxidation reactions in the temperature range between 570 K and 720 K provide the required heat for evaporation.

In a 500 h long-term test with light fuel oil (sulphur content $\zeta s = 5$ wt. ppm), the successful operation of the fuel processor was demonstrated. By implementing periodic catalyst regeneration cycles, the initial performance of the reactor could be achieved even after 500 h of operation generating a hydrogen yield of over 72 vol.% (dry).

3.2. Investigations on a small scale reactor

3.2.1. Materials and methods

The small scale reformers (SSR) are used in order to optimise the full scale reformer (FSR). Similar to the full scale reformer they are designed as catalytically coated plate heat exchangers coupling thermally the reforming reaction with a catalytic combustion. Optimisation tests of the SSR are carried out with respect to the flow field geometry and the reformer catalyst. To guarantee a similar behaviour of small scale and full scale reformers, the down scaling is accomplished by reducing the number of heat exchanger plates and maintaining the plate geometry. For the SSR the thermal power input is $P_{th} = 1$ kW resulting in a gas hourly space velocity (GHSV) equal to 25,000 h^{-1} at a steam to carbon ratio (SCR) equal to 4. Similar to the FSR the SSR includes one plate for solid phase temperature measurements (see Fig. 4). In addition, temperatures are measured at the reformer inlet and outlet and burner.

For the tests a fuel mixture of Shellsol A 100 (20 wt.%) and Shellsol D 100 (80 wt.%) was used. The diesel surrogate obtained had a chemical formula of $C_{14.37}H_{27.40}$ and is comprised of the fractions summarised in Table 1.

Operating the SSR, water and fuel are evaporated separately before being mixed at around 673 K and being superheated rapidly to a temperature of 923 K in order to prevent carbon/coke formation upstream of the reformer. The reformer was heated by hydrogen

Table 1
Diesel surrogate composition.

Fraction	Value	Unit	Method of analysis
Paraffins	48	wt.%	GC
Naphthenes	32	wt.%	GC
Aromatics	20	wt.%	SMS 2728
Benzenes	5	wt. ppm	GC
Sulphur	<2	wt. ppm	SMS 1897

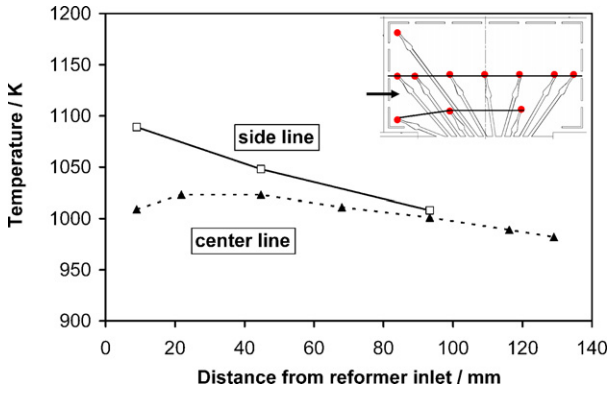

Fig. 5. Plate temperatures at set temperature 1023 K and SCR equal to 4.

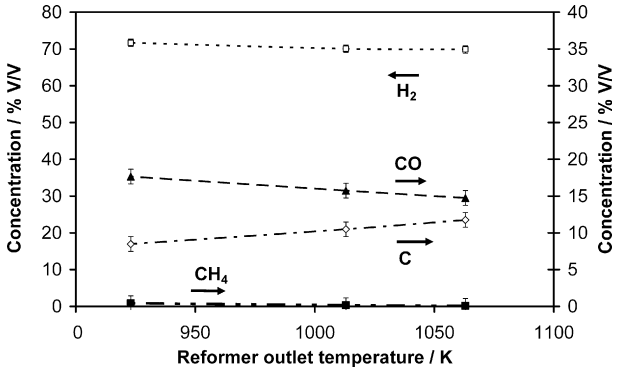

Fig. 6. Dry reformate gas concentrations at SCR equal to 4.

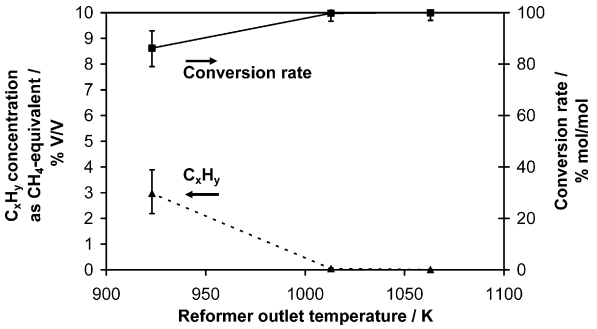

Fig. 7. Residual hydrocarbons and conversion rate at SCR equal to 4.

combustion on the combustion side. To control the operating temperature of the reformer, measuring point no.6 on the temperature measurement plate (see Fig. 3) was found to be the point with the highest temperature on the centre line.

In the presented test series the FSR flow field was maintained for the SSR and the reference catalyst from the FSR was applied. For the reformer testing a test program was executed varying the SCR between 3 and 4 at set temperatures 1073 K, 1023 K, and 973 K. Operating points were maintained for 2 h each to guarantee steady state operation. The reformate gas was continuously analysed measuring: hydrogen (H_2) concentrations by thermal conductivity detector, carbon monoxide (CO), carbon dioxide (CO_2), and methane (CH_4) concentrations by infrared analysis, and unconverted hydrocarbons (C_xH_y) by flame ionisation detection (FID).

4. Results

Fig. 5 shows the solid phase temperatures measured in the reformer operation at set temperature of 1023 K. The temperatures are decreasing with rising distance from the reformer inlet since hydrogen combustion takes place close to the inlet of the reformer due to its high reaction rate. High temperatures occur on the side line since an impinging stream is provoked by the burner side inlets.

Fig. 6 describes dry reformate gas concentrations after condensation at 278 K for reformer outlet temperatures between 923 K and 1073 K. Hydrogen yields of approximately 70 vol.% are achieved decreasing slightly for higher reformer temperatures. The tested steam reforming catalyst also promoted the water gas shift reaction (WGS). Evidently, the decrease of the hydrogen yield goes along with a decrease of the carbon dioxide and an increase of carbon monoxide, revealing that the WGS is constrained at higher temperatures. The residual hydrocarbon concentration is decreasing with high temperatures, indicating that the reforming reaction only performed sufficiently at temperatures from 1013 K at the reformer outlet (see Fig. 7). The fuel conversion rate calculated from the reformate gas composition exceeded 99.5% at reformer outlet temperatures above 1013 K. At an outlet temperature of 923 K a fuel conversion rate of 86.2% only could be achieved.

For every operation point of the catalyst test program a reformate gas sample was analysed by gas chromatography (GC) after condensation at 278 K. The GC allows the detection of gaseous hydrocarbons with carbon numbers up to 5. In Fig. 8 (left) the detected species are described for a reformer temperature variation at a SCR equal to 4. At reformer outlet temperatures above 1013 K only methane was detected in the reformate gas. The concentration increases with decreasing temperature as the reforming reaction is constrained and the fuel conversion rate falls. At 923 K ethane, ethene, and propane occurred additionally which agrees with the observation made in Fig. 7 that total hydrocarbon concentration was much higher or conversion rate was low at that temperature. The second diagram in Fig. 8 (right) shows the hydrocarbon species detected at a constant set temperature equal to 1013 K and

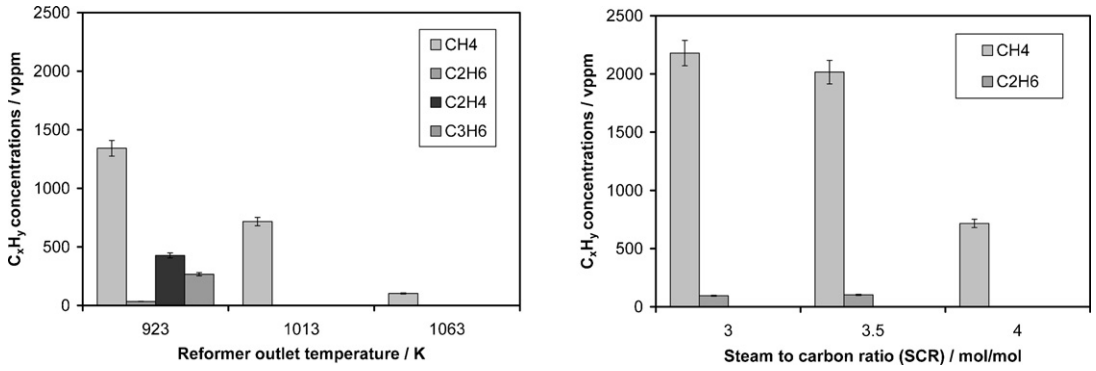

Fig. 8. Left: dry reformate gas concentrations at SCR 4; right: dry reformate gas concentrations at set temperature 1013 K.

Table 2
Validation cases, conditions.

	Case		
	1 [16]	2 [16]	3 (Section 3.1)
P_{th}, reformer inlet	10 kW	4 kW	6 kW
P_{th}, burner inlet	4.25 kW	2.5 kW	3.8 kW
SCR	4	4	4.4
Air ratio, λ	2.25	2	3.4
Inlet temperature reformer	873 K	640 K	733 K
Inlet temperature burner	573 K	573 K	613 K
Fuel reformer	Shellsol surrogate	Shellsol surrogate	Low sulphur fuel oil, 6 wt. ppm sulphur, long term test
Catalyst activity, α	100%	100%	3%

a variation of the SCR. Mainly methane was detected whose concentrations increased with decreasing SCR. At a SCR equal to 3 also ethane occurred in the reformate gas with a concentration equal to 32 vppm. Based on these results the lower operational limit value for the SCR can be set to 3.5 and for the reformer temperature to 1013 K.

5. Computational results and discussion

5.1. Validation

Before starting with the computation of design variations CFD results of calculations are compared to experimental results of the 10 kW reformer. Fig. 9 shows the corresponding outline of the validation case with the position of inlets and outlets.

In Table 2 the conditions of the regarded validation cases are listed. Case no. 1 and 2 were measured by Wruck [16]. Reformer reactant was Shellsol surrogate as mentioned in Section 3.2. Since the fuel contains less than $\zeta_s < 2$ wt. ppm sulphur catalyst activity α, given by the following equation, remains unaffected:

$$\alpha = \frac{S}{S_0} \tag{12}$$

Assuming an uniform catalyst activity and uniform deactivation the rate constant k_0 related to the mass of catalysts are corrected with the catalyst activity α is given by:

$$k_0^* = k_0 \alpha \tag{13}$$

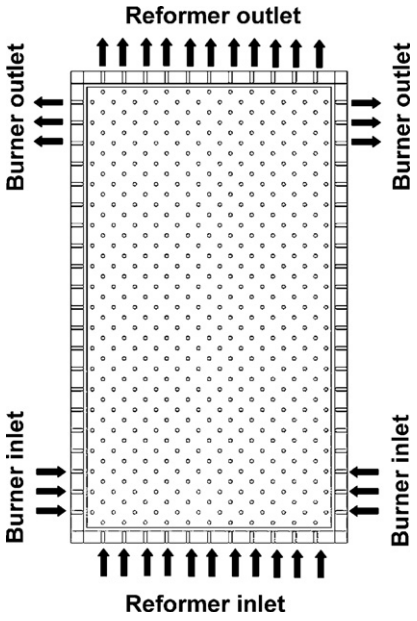

Fig. 9. Outline of current reactor.

The catalyst activity was determined indirectly by computation of variations.

In all cases the SCR of the reformer reactants is about 4 and a low sulphur fuel oil containing $\zeta_s = 5$–6 wt. ppm sulphur was supplied to the burner. In contrast to the first two variations a low sulphur fuel oil was used in the reformer. Beyond that the air ratio was increased to $\lambda = 3.4$. Due to the fact that the experiment no. 3 (see Section 3.1) was a long term test with low sulphur fuel oil and with an unadapted regeneration strategy the catalyst activity falls to 3%. Beyond that the used catalyst was not optimised for a fuel containing sulphur.

Fig. 10 shows the temperature distribution in the plate and fuel mass fractions in the reformer and burner for case no. 1. Especially at low air ratios the simple lateral inlet for the burner leads to a hot outer region. Since the reaction rate of the steam reforming reaction is supported by high reactor temperature only in the middle of the reactor plate hydrocarbon reaches the outlet. The amount of fuel at the outlet corresponds to a fuel conversion of $X = 92\%$. Due to a relative low reactor outlet temperature of $T = 973$ K a full conversion in the reformer was not achieved.

The computational results are validated with the measured temperature distribution in the reactor and fuel conversion in the reformer shown in Fig. 11. In all cases the same fuel conversion was reached. The agreement of the temperatures on the central line is very good for case 1 and 3. In case 2 a maximum deviation of 23 K can be observed. Considering the error of thermocouples this result is satisfactory. The temperatures on the outer lines are also in a good agreement with a maximum absolute deviation of 24 K. First calculation with a more complex reaction mechanism for the combustion with homogenous reactions a temperature distribution closer to the measured values can be found. The measured values at the burner inlets differ in some case. One possible reason is a different coating at these places. On grounds of low catalyst activity in case 3 a conversion of just $X = 67\%$ was observed.

5.2. Variation of geometry

The aim of the computational investigation is the optimisation of performance and durability of the reactor. The following criteria are stated:

- Fast overheating of reformer reactants to reduce coke formation.
- High fuel conversion rates in the reformer.
- Homogenous temperature distribution to prevent material damages.
- Maximum temperature below operating temperature limit $T = 1173$ K.
- Low pressure loss in the burner to increase system efficiency.

In the framework of the numerical investigation the following geometry variations are rated on the basis of the computational results of case 3 and case 1 with increased outlet temperature $T = 1023$ K:

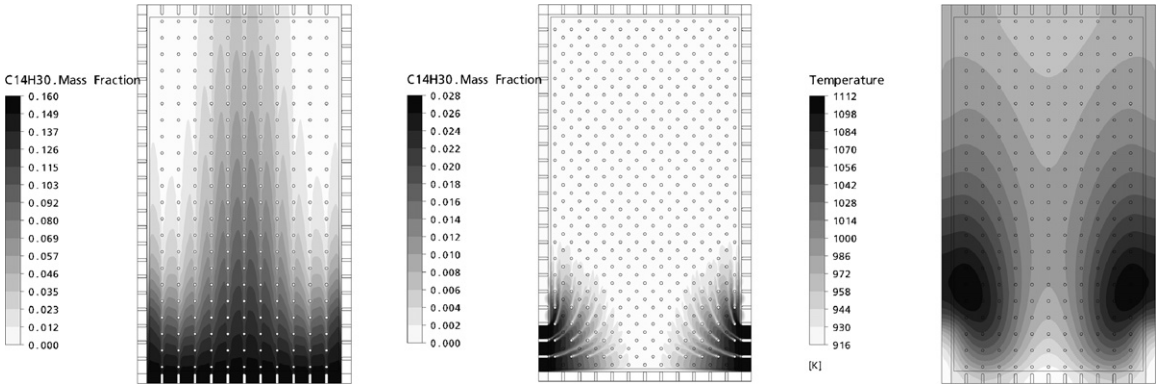

Fig. 10. Computation results, current reactor, case 1, fuel mass fraction reformer (left) and burner (middle), temperature in the plate (right).

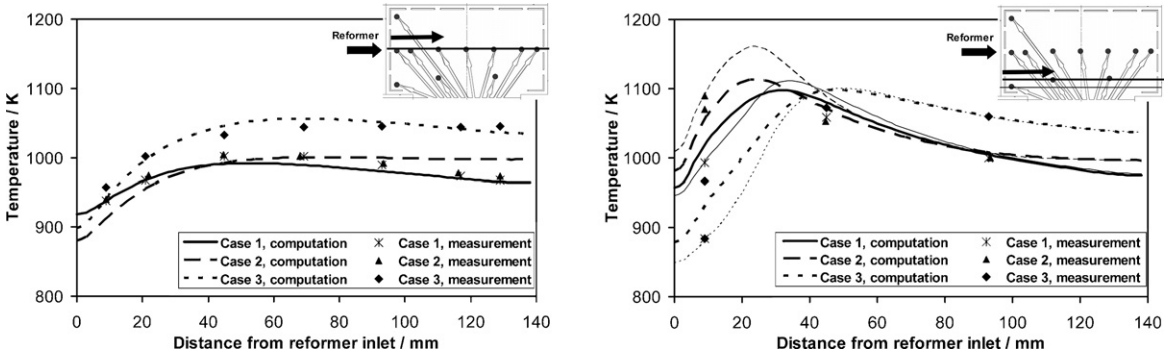

Fig. 11. Comparison of temperature distribution in reactor, current reactor, cases 1–3, measurements and computational results, central line (left) and outer lines (right).

- Current reactor.
- Current reactor with increased channel height.
- Current reactor with increased burner inlet width.
- Current reactor with reduced burner inlet width.
- Current reactor with switched sides (reformer and burner).
- S-flow reactor.
- Cross flow reactor.
- Counter flow reactor based on the current reactor.
- Parallel flow reactor with supply of burner reactants through multiple holes.
- Parallel flow reactor with switched sides (reformer and burner).

Fig. 12 shows the computational results of the cross flow reactor. Since the heat demand and heat source do not match, a hot spot appears at top left. The standard deviation of solid phase temperature for case 3 and the cross flow reactor is 100 K (see Fig. 13). The calculation of the current reactor and the same conditions result in a deviation of just 60 K. A standard deviation of 81 K and 117 K is observed for S-flow and the counter flow reactor. Furthermore, operating temperature limit is exceeded for counter flow and cross flow reactor. Table 3 presents a rating matrix regarding the geometry variations. The current reactor with switched sides has a good performance with conditions referring to case 3, but at low air ratios as in case 1 the maximum temperature is exceeded and standard deviation of 91 K is reached. In the current reactor and for case 3 the reformer reactants are heated up to $T = 973$ K in the range up to 15 mm of the reactor length. By increasing the burner inlet width by 50% the length for reactants overheating rises by 40% and vice versa. So, smaller inlets are favoured for reactant overheating. By increasing channel height from 0.6 mm up to 0.8 mm the pressure loss in the burner is reduced by 55%.

For high air ratios referring to case 3 the parallel flow reactor with supply of burner reactants through multiple holes has no advantages over the current reactor. Rather than that, the length for

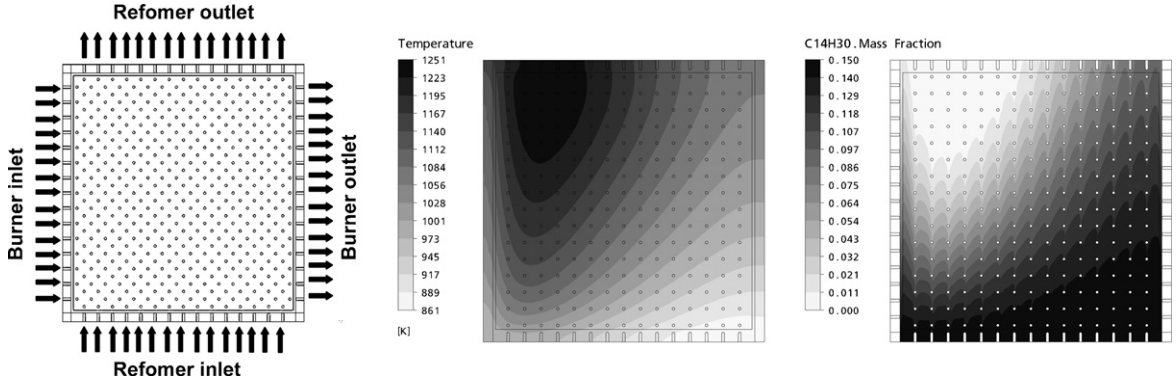

Fig. 12. Computational results cross flow reactor, case 3, outline (left), temperature in the plate (middle), fuel mass fractions reformer (right).

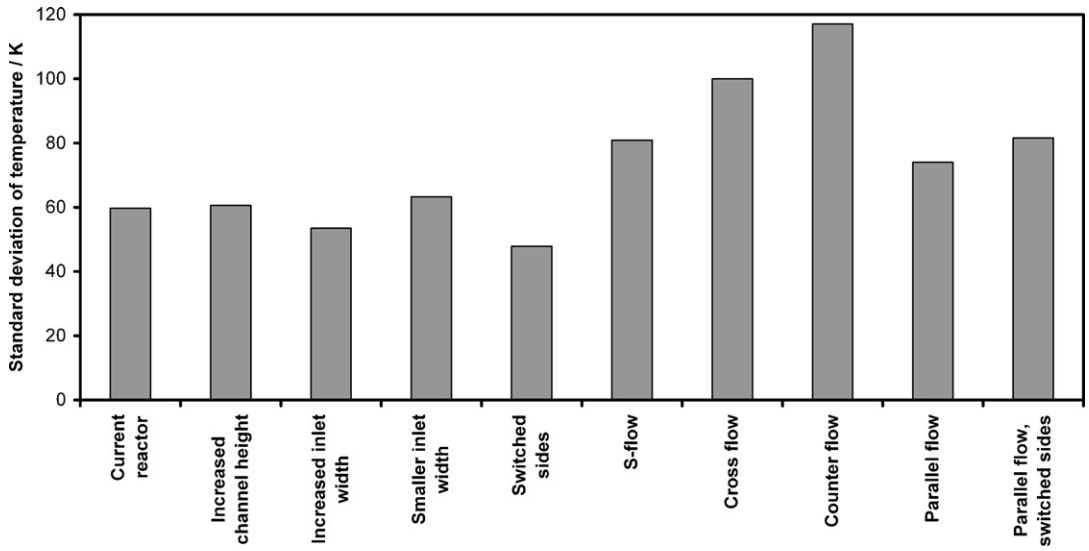

Fig. 13. Standard deviation of temperature, case 3, geometry variations.

Table 3
Rating matrix geometry variations: 0, does not meet demands; 10, meet demands perfectly; 0*, exceeded temperature limit lead to drop of rating; C3, case 3; C1, case 1 with increased reactor outlet temperature 1023 K and reduced catalyst activity 3%.

Criteria	Overheating reformer reactants		Conversion reformer		Homogeneity temperature		Maximum temperature		Pressure loss burner		Total	
Weighting	0.3		0.35		0.2		0.1		0.05		1	
Conditions	C3	C1	C3	C1	C3	C1	C3	C1	C3	C1	C3	C1
Current reactor	7	9	1	4	5	4	8	1	7	9	4.6	5.5
Increased channel height	7	9	1	4	4	5	9	2	10	10	4.7	5.8
Increased inlet width	6	–	1	–	5	–	8	–	8	–	4.3	–
Smaller inlet width	8	10	1	4	4	5	8	2	5	8	4.6	6
Switched sides	7	10	2	3	6	1	8	0	8	9	5.2	0*
S-flow	6	–	1	–	2	–	8	–	2	–	3.5	-
Cross flow	3	–	5	–	0	–	0	–	10	–	0*	–
Counter flow	5	–	9	–	0	–	0	–	6	–	0*	–
Parallel flow	5	9	1	4	3	5	8	4	8	10	3.7	6
Parallel flow, switched sides	5	7	1	3	2	6	8	4	6	7	3.4	5.1

reactant overheating increases by 57% as shown in Fig. 14. The conversion of fuel is reduced by 3%. However, at low air ratio (case 1) the maximum solid phase temperature in the parallel flow reactor is below the value in the current reactor. Therefore the parallel flow reactor permits lower air ratios without exceeding the operating temperature limit.

In contrast to the current reactor the complexity and costs of the parallel flow reactor is higher.

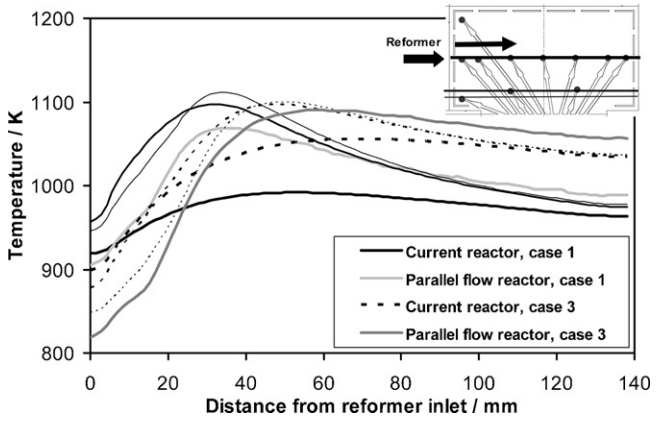

Fig. 14. Calculated temperature distribution in the reactor, current reactor and parallel flow reactor, case 1 and case 3.

Therefore additional CFD simulations are performed to compare these two parallel flow concepts under different conditions. For this a variation of one parameter in each case is put into effect. The conditions at reference point are given in Table 4. An idealised 2D parallel flow reactor was used for this computational study.

Fig. 15 shows the result of these parameter variations. By increasing the outlet temperature via thermal input in the burner the level of temperature is increased in the whole reactor for both parallel flow concepts (see Fig. 15a). However, only in the current reactor the operating temperature limit is exceeded. For increased air ratio $\lambda = 3$ the temperature distribution in the reactor are homogenised in both cases (see Fig. 15b). In contrast to the previous computations the length of superheating reformer reactants in the parallel flow reactor is shorter than in the current reactor. The difference between these calculations is the higher catalyst activity in the reformer and the idealised parallel flow reactor. By decreasing the catalyst activity the reactor temperatures rise about a fix

Table 4
Conditions at reference point.

P_{th}, reformer inlet	10 kW
Reactor outlet temperature	1023 K
SCR	4
Air ratio, λ	2
Inlet temperature reformer	773 K
Inlet temperature burner	573 K
Catalyst activity, α	100%

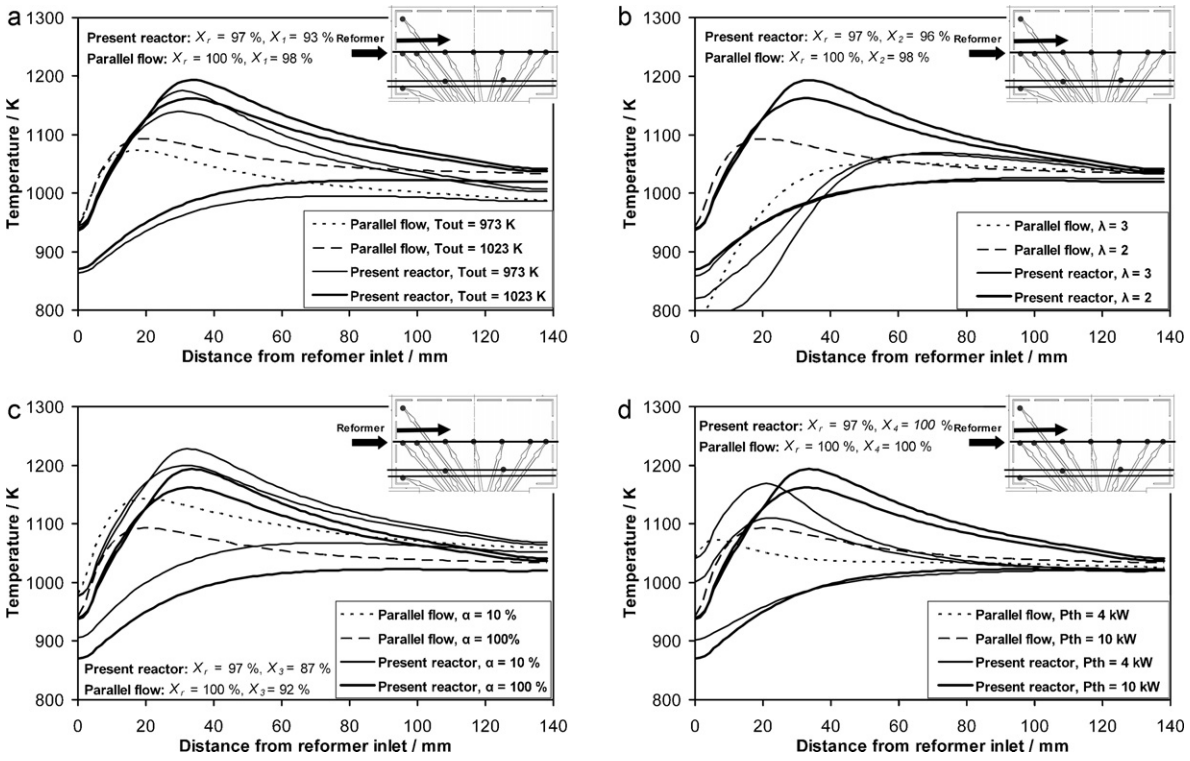

Fig. 15. Parameter variation calculation, current reactor and ideal parallel flow reactor, variation of reactor outlet temperature (top left, (a)), variation of air ratio (top right, (b)), variation of catalyst activity (bottom left, (c)), variation of thermal power supply reformer (bottom right, (d)).

value (see Fig. 15c). A lower reformer inlet power leads to lower reactor temperatures (see Fig. 15d). At the reference point conversion rates of X_r = 100% and X_r = 97% are calculated for the parallel flow reactor and the current reactor. By decreasing the outlet temperatures to T_{out} = 923%. The conversion rate drops to X_1 = 93% for the current reactor. This effect was also observed in the framework of the experiments performed on the small scale reactor (see Section 3.2).

The observed hot spots in the current concept were also theoretically examined by Gritsch [1]. He investigated the conduction of flow in catalytically coated plate heat exchanger for coupled methane steam reforming and methane combustion. During computational investigations he found out that hot spots can occur in a counter flow reactor. In a parallel flow reactor heat source and heat sink are more balanced. Gritsch mentioned that a multistage supply of fuel on the combustion side enhances the reactor performance.

The unfavourable temperature distribution of a counter flow reactor is confirmed by this work. Furthermore, the result of the numerical study is that two different parallel flow concepts best meet the demands. Referring to the stated requirements for the performance of a steam reformer the parallel flow reactor with multiple holes and the current reactor provide a more homogenous temperature distribution and a faster reformer reactants overheating than the cross flow, S-flow and counter flow concepts. Beyond that the temperature distribution in the parallel flow reactor depends on the following conditions:

- Design of parallel flow reactor.
- Catalyst activity.
- Thermal input.
- Air ratio.

The current reactor with increased channel height and the reactor with reduced burner inlet width also achieve the best rating results. The reasons are the reduced pressure loss in the first case and the enhanced reactants overheating the second case.

6. Conclusions

- Experimental tests were performed on a 10 kW steam reformer and a small scale reformer for fuel oil and diesel fuel.
- The experimental results show that the reformer design applied for the validation allows inlet temperatures below 773 K because of its internal superheating capability.
- CFD computation reproduces the measured temperature field in the reactor.
- Comparable results (temperature profiles) are presented for the numerical and experimental data considering three different operating points.
- The aim of geometry optimisation is enhanced reactant overheating of reformer reactants, conversion of fuel in the reformer, homogeneity of solid phase temperatures and lower pressure loss in the burner.
- The present reactor (parallel flow with lateral inlets) with reduced burner inlet width or/and increased channel height best meets demands.
- For low air ratios the parallel flow reactor shows an improved performance in comparison to the reference system. However, in some cases the time for reactant overheating on the reformer side increases.

Acknowledgement

This research and development project is funded by the German Federal Ministry of Economics and Technology (BMWi, FKZ 0327724).

References

[1] A. Gritsch, Wärmeintegrierte Reaktorkonzepte für katalytische Hochtemperatur-Synthesen am Beispiel der dezentralen Dampfreformierung von Methan, PhD-Thesis, Universität Stuttgart, 2008.
[2] G. Kolb, J. Schürer, D. Tiemann, M. Wichert, R. Zapf, V. Hessel, H. Löwe, Fuel processing in integrated microstructured heat-exchanger reactors, J. Power Sources 171 (2007) 198–204.
[3] J. Thormann, Diesel-Dampfreformierung in Mikrostrukturreaktoren, PhD-Thesis, Universität Clausthal, 2009.
[4] J. Xu, G.F. Froment, Methan steam reforming: II. Diffusional limitations and reactor simulation, AIChE J. 35 (1989) 97–103.
[5] Z. Chen, Y. Yan, S.S.E.H. Elnashaie, Hydrogen production and carbon formation during the steam reformer of heptane in a novel circulating fluidized bed membrane reformer, Ind. Eng. Chem. Res. 43 (2004) 1323–1333.
[6] M.A. Rakib, J.R. Grace, S.S.E.H. Elnashaie, C.J. Lim, Y.G. Bolkan, Kinetic simulation of a compact reactor system for hydrogen production by steam reforming of higher hydrocarbons, Canad. J. Chem. Eng. 86 (2008) 403–412.
[7] J.R. Rostrup-Nielsen, L.J. Christiansen, J.H. Bakhansen, Activity of steam reforming catalysts: role and assessment, Appl. Catal. 43 (1988) 287–303.
[8] P.B. Tottrup, Evaluation of intrinsic steam reforming kinetic parameter from rate measurements on full particle size, Appl. Catal. 4 (1982) 377–389.
[9] J.R. Rostrup-Nielsen, Catalytic steam reforming, in: J.R. Anderson, M. Boudart (Eds.), Catalysis Science and Technology, vol. 5, Springer Verlag, Berlin, 1984, pp. 1–118.
[10] R.E. Hayes, S.T. Kolaczkowski, Introduction to Catalytic Combustion, Gordon and Breach Science Publisher, Amsterdam, 1997.
[11] L.D. Pfefferle, W.C. Pfefferle, Catalysis in combustion, Catal. Rev. Sci. Eng. 29 (1987) 219–267.
[12] Y.F.Y. Yao, Oxidaton of alkanes over noble metal catalysts, Ind. Eng. Chem. Prod. Res. Dev. 19 (1980) 293–298.
[13] E.A. Mason, A.P. Malinauskas, Gas Transport in Porous Media: The Dusty- Gas Model, Elsevier, New York, 1983.
[14] J.C. Gottifredi, E.E. Gonzo, O.D. Quiroga, Effectiveness factor calculation, in: S. Whitaker, A.E. Cassano (Eds.), Chemical Reactor Concept and Design, Gordon and Breach Science Publisher, New York, 1986.
[15] ANSYS CFX 11.0 flow solver manual, Ansys Inc., Canonsburg, 2006.
[16] R. Wruck, Beitrag zur Brenngaserzeugung mittels Dampfrefomierung von Heizöl EL schwefelarm für die Nutzung in Niedertemperatur-PEM-Brennstoffzellen, PhD Thesis, RWTH Aachen, 2010.